

Photonic crystal slabs for surface contrast enhancement in microscopy of transparent objects

Yousef Nazirizadeh,^{1,*} Tim Becker,² Julia Reverey,³ Christine Selhuber-Unkel,³ Daniel H. Rapoport,² Uli Lemmer,⁴ and Martina Gerken¹

¹*Institute of Electrical and Information Engineering, Christian-Albrechts-Universität zu Kiel, D-24143 Kiel, Germany*

²*Fraunhofer Institute for Marine Biotechnology, D-23562 Lübeck, Germany*

³*Institute for Materials Science, Christian-Albrechts-Universität zu Kiel, D-24143 Kiel, Germany*

⁴*Light Technology Institute and Center for Functional Nanostructures (CFN), Karlsruhe Institute of Technology (KIT), D-76131 Karlsruhe, Germany*

*yn@tf.uni-kiel.de

Abstract: In optical microscopy the contrast of transparent objects achieved with conventional methods is often not satisfactory, for example for the automated recognition of cells. In this paper we present a nano-optical label-free approach for contrast enhancement based on photonic crystal slabs (PCS) as the specimen holder. Quasi-guided modes inside these structures cause an intrinsic color of the PCS, which strongly depends on the wavelength and the quality factor of the optical mode. Objects on the surface of the PCS experience a significant color and intensity contrast enhancement, as they change properties of the optical modes.

©2012 Optical Society of America

OCIS codes: (170.0180) Microscopy; (160.5298) Photonic crystals; (170.1530) Cell analysis.

References and links

1. D. J. Stephens and V. J. Allan, "Light microscopy techniques for live cell imaging," *Science* **300**(5616), 82–86 (2003).
2. I. L. Medintz, H. T. Uyeda, E. R. Goldman, and H. Mattoussi, "Quantum dot bioconjugates for imaging, labelling and sensing," *Nat. Mater.* **4**(6), 435–446 (2005).
3. F. Zernike, "Phase contrast, a new method for the microscopic observation of transparent objects," *Physica* **9**(7), 686–698 (1942).
4. R. D. Allen, G. B. David, and G. Z. Nomarski, "The zeiss-Nomarski differential interference equipment for transmitted-light microscopy," *Z. Wiss. Mikrosk.* **69**(4), 193–221 (1969).
5. J. Itten, *Kunst der Farbe* (Otto Maier Verlag, 1961).
6. A. S. G. Curtis, "The mechanism of adhesion of cells to glass: a study by interference reflection microscopy," *J. Cell Biol.* **20**, 199–215 (1964).
7. B. Rothenhäusler and W. Knoll, "Surface-plasmon microscopy," *Nature* **332**(6165), 615–617 (1988).
8. K. Giebel, C. Bechinger, S. Herminghaus, M. Riedel, P. Leiderer, U. Weiland, and M. Bastmeyer, "Imaging of cell/substrate contacts of living cells with surface plasmon resonance microscopy," *Biophys. J.* **76**(1), 509–516 (1999).
9. B. Polisky, R. Jenison, S. Yang, and A. Haerberli, "Interference-based detection of nucleic acid targets on optically coated silicon," *Nat. Biotechnol.* **19**(1), 62–65 (2001).
10. R. Jenison, M. Rihaneck, and B. Polisky, "Use of a thin film biosensor for rapid visual detection of PCR products in a multiplex format," *Biosens. Bioelectron.* **16**(9-12), 757–763 (2001).
11. B. P. Möhrle, K. Köhler, J. Jaehrling, R. Brock, and G. Gauglitz, "Label-free characterization of cell adhesion using reflectometric interference spectroscopy (RIFS)," *Anal. Bioanal. Chem.* **384**(2), 407–413 (2005).
12. S. Fan and J. Joannopoulos, "Analysis of guided resonances in photonic crystal slabs," *Phys. Rev. B* **65**(23), 235112 (2002).
13. Y. Zhao, X. Zhao, and Z. Gu, "Photonic crystals in bioassays," *Adv. Funct. Mater.* **20**(18), 2970–2988 (2010).
14. B. T. Cunningham, P. Li, S. Schulz, B. Lin, C. Baird, J. Gerstenmaier, C. Genick, F. Wang, E. Fine, and L. Laing, "Label-free assays on the BIND system," *J. Biomol. Screen.* **9**(6), 481–490 (2004).
15. Y. Nazirizadeh, U. Bog, S. Sekula, T. Mappes, U. Lemmer, and M. Gerken, "Low-cost label-free biosensors using photonic crystals embedded between crossed polarizers," *Opt. Express* **18**(18), 19120–19128 (2010).
16. S. M. Shamah and B. T. Cunningham, "Label-free cell-based assays using photonic crystal optical biosensors," *Analyst (Lond.)* **136**(6), 1090–1102 (2011).

17. Y. Nazirizadeh, J. Müller, U. Geyer, D. Schelle, E.-B. Kley, A. Tünnermann, U. Lemmer, and M. Gerken, "Optical characterization of photonic crystal slabs using orthogonally oriented polarization filters," *Opt. Express* **16**(10), 7153–7160 (2008).
 18. Y. Nazirizadeh, J. G. Müller, U. Geyer, U. Lemmer, and M. Gerken, "Direct observation of photonic modes in photonic crystal slabs," in *Proceedings of International Conference on Transparent Optical Networks* (Academic, 2008), pp. 72–75.
 19. Y. Nazirizadeh, U. Lemmer, and M. Gerken, "Surface contrast microscopy," in *Novel Technologies in Microscopy* (2011), Vol. 65, paper NTuC3.
 20. J. L. Guo, "Nanoimprint lithography: methods and material requirements," *J. Adv. Mater.* **19**(4), 495–513 (2007).
 21. A. S. Curtis, B. Casey, J. O. Gallagher, D. Pasqui, M. A. Wood, and C. D. Wilkinson, "Substratum nanotopography and the adhesion of biological cells. Are symmetry or regularity of nanotopography important?" *Biophys. Chem.* **94**(3), 275–283 (2001).
 22. A. Michelson, *Studies in Optics* (University of Chicago Press, 1927).
 23. W. D. Wright, "A re-determination of the trichromatic coefficients of the spectral colours," *Trans. Opt. Soc.* **30**(4), 141–164 (1929).
 24. D. L. MacAdam, "Visual sensitivities to color differences in daylight," *J. Opt. Soc. Am.* **32**(5), 247–273 (1942).
 25. I. D. Block, P. C. Mathias, S. I. Jones, L. O. Vodkin, and B. T. Cunningham, "Optimizing the spatial resolution of photonic crystal label-free imaging," *Appl. Opt.* **48**(34), 6567–6574 (2009).
 26. D. H. Rapoport, T. Becker, A. Madany Mamlouk, S. Schickanz, and C. Kruse, "A novel validation algorithm allows for automated cell tracking and the extraction of biologically meaningful parameters," *PLoS ONE* **6**(11), e27315 (2011).
-

1. Introduction

Since the invention of the microscope optimizing the contrast of transparent specimens is an important issue for imaging samples that do not strongly absorb light. This is in particular the case for the visual recognition of bacteria and unicellular organisms. Today, a variety of label-based and label-free contrast enhancement methods [1–4] is available, which allows for a sufficient contrast for visual inspections. In contrast, for applications that require an automated image processing, such as cell colony analyses and cell adhesion studies, the obtained contrast is often unsatisfactory and leads to high error rates. Generally, the contrast of an image is not only a mathematical definition, but also is composed of emotional components. This was first described by J. Itten in his theory of contrast [5], where he introduced the Itten's seven contrasts. According to him two of the most important types of contrast are the contrast of hue and the contrast of intensity, both used in today's contrast enhancement techniques. In staining and fluorescence tagging methods stains or dyes are incorporated into the tissue and cause a combination of contrast of hue and intensity. These methods in particular are suitable for histological specimens, where specific labels enable differentiating of degenerate cells in a cell colony or sub-cellular components. Most of these labels, however, are toxic to the organism and hence are limited in their application fields. Nowadays also living cells can be transfected with fluorescent dyes. However, this is often cost- and time-consuming and not suitable for high-throughput experiments. Since the invention of phase contrast microscopy [3], differential interference contrast microscopy [4], and interference reflection microscopy [6] label-free methods are a standard in laboratories and allow for a broad field of use. Alternative approaches are surface based contrast enhancement methods. In surface-plasmon microscopy [7, 8] surface plasmon resonances (SPRs) provided by a metal film on top of the specimen holder are used to reveal interactions of the object with the surface. For the excitation of these resonances prisms are used, which lead to non-standard optical setups and additional costs. Another surface based method uses interferences in thin films, which cause intensity modulations in the transmission spectrum. Any object on the thin film surfaces changes these modulations and leads to a color change. There have been investigations on biomolecular interactions [9, 10] and on cells [11] using this technique. Although the optical setup of this method is very simple, the obtained contrast of hue is small, as the intensity modulations in the spectrum extend over the entire visible spectrum. In a lateral view, thin films of a high refractive index on a low refractive index substrate are waveguides with discrete guided modes of relatively limited spectral width. These guided modes, however, cannot couple to the far field and hence are not visible in transmission or reflection measurements.

2. Photonic crystal slabs as the specimen holder

According to Bragg's theory, a suitable periodic nanostructure in a thin film waveguide causes scattering of guided modes to the far field and vice versa. These modes are referred to as quasi-guided modes (QGMs) (Fig. 1(a)) and are the origin of so-called guided-mode resonances (GMRs), which appear in the transmission or reflection spectra superimposed with thin film interferences (Fig. 1(b)) [12]. The central wavelengths of these resonances are proportional to the periodicity of the nanostructure and the effective refractive index of the QGM. Therefore, nanostructured thin films, which are also called photonic crystal slabs (PCSs), respond very sensitively to refractive index changes on their surface. Any change in refractive index leads to a change in the effective refractive index of the QGM and as a consequence of the Bragg condition the spectral position of the mode is changed. As the GMR is directly related to the QGM, its spectral position is changed, too. A further property of the GMR, which is affected by a refractive index change, is its quality factor, which is inversely proportional to the line width of the resonance. Using a spectrometer, today GMRs are used in various biological applications ranging from biosensors [13–15] to cell analysis [16]. However, in a visual transmission experiment with a white light source, as used in many light microscopes, the GMRs do not induce any specific color or intensity changes. This is because of the superposition with the white background light passing the PCS as well (Fig. 1(b)). We use polarization filters before and behind the PCS as shown in Fig. 1(a) to suppress the background white light source [17]. Only the fraction of light, which couples to the QGM inside the PCS, undergoes a polarization rotation and can pass the second polarization filter. For a maximization of this effect the orientation of the PCS relative to the crossed polarization filters should be at 45° for a linear PCS [18]. In this configuration only the GMRs are observed in the transmission spectrum (Fig. 1(b)). This has two significant consequences for transmission experiments. First, the PCS's surface appears in an intrinsic color depending on the spectral position of the GMR, as these resonances are spectrally limited. Thus, any spectral shift results in a color shift of the PCS. Second, the spectrally integrated intensity is only a function of the GMR's spectral line-width. Hence, any change in the line-width results in an intensity change in the image. We propose to employ these two effects for contrast enhancement using the contrast of hue and the contrast of intensity and refer to this method as surface contrast microscopy [19]. With microscope slides functionalized with PCSs and two polarization filters in the optical path this method is fully integratable into conventional light microscopes. Furthermore, today there are fabrication methods available, which allow for a large-area and cost-efficient production of PCSs [20]. To exclude that living cells are influenced by the nano-topography of the surfaces [21], the PCS surface can be planarized with an optically inactive passivation layer. In this work, however, we used non-planarized PCSs.

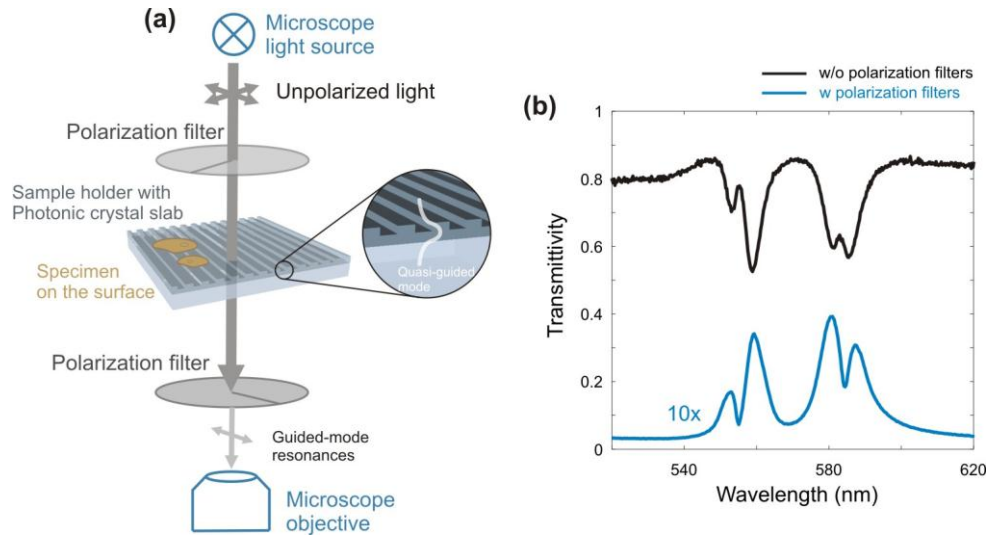


Fig. 1. (a) Schematic setup for surface contrast microscopy (SCM). Two polarization filters before and behind the photonic crystal slab (PCS) suppress background light and allow only guided-mode resonances (GMR), which have their origin in the quasi-guided modes, to pass. Any object on the surface influences the optical properties such as resonance position and quality factor of the GMR, which leads to a contrast of hue and intensity. (b) Transmission through a PCS with and without crossed polarization filters. The PCS is a 70-nm deep linear grating etched into a 300-nm Ta_2O_5 layer on a glass substrate and has a periodicity of 370 nm. Without polarization filters the transmission spectrum is a superposition of the white background light and the GMRs. Here the GMRs do not induce any significant color or intensity changes. With polarization filters only the GMR can pass the second polarization filter and hence any change in optical properties of the GMR is visible in the transmission image.

3. Refractometric investigations on the photonic crystal slabs

Since the refractive index change on the surface of the PCS is the origin of the contrast enhancement we investigate in Fig. 2 the influence of the refractive index on the GMRs. We tuned the refractive index using air and blends of water and glycerol. The PCS used here was composed of a 300 nm Ta_2O_5 layer on a glass substrate with a 70 nm deep linear grating. The periodicity of this structure was 370 nm. In Fig. 2(a) we plot the transmission spectrum with crossed polarization filters against the refractive index. As expected, we observe two main phenomena. First, all resonances shift towards longer wavelengths with higher refractive indices. This is the origin of the contrast in hue, which can be seen in the lower part of Fig. 2(a), where the color of the PCS changes from yellow to red. Second, the spectrally integrated transmission intensity decreases. This is due to an increase in the quality factor of all resonances with higher refractive indices. The quality factor is the central wavelength of the resonance divided by its linewidth. The overall contrast is a superposition of the hue contrast and the intensity contrast.

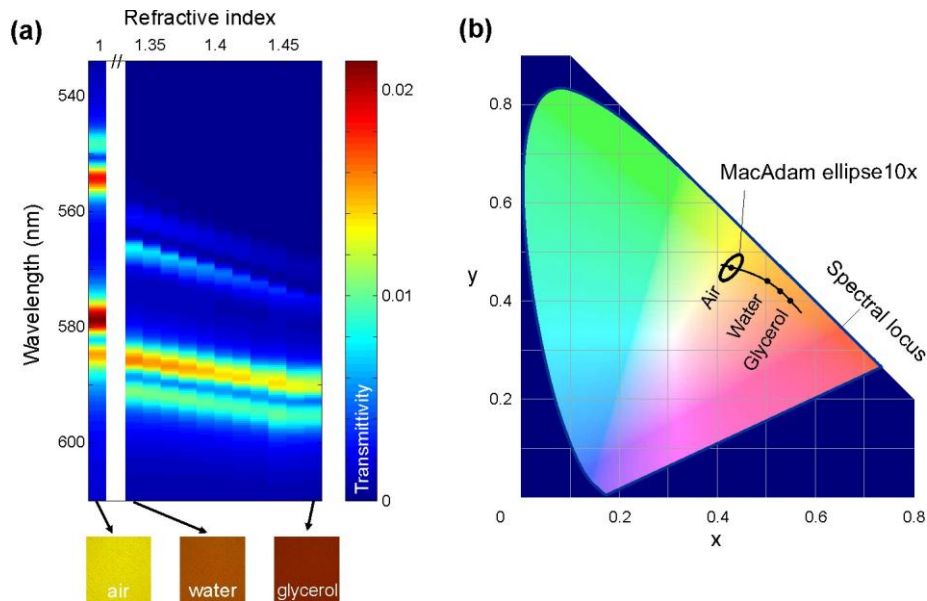


Fig. 2. Refractometric experiments with PCSs. (a) Transmission spectra with crossed polarization filters of the PCS with varying bulk refractive index (air and water-glycerol dilutions). A spectral position shift and a decrease in intensity are observed. (b) The color change caused by the spectral position shift is plotted in the CIE color space. A shift from yellow to red is observed. A 10x magnified MacAdam ellipse around the color point for air indicates the loci, which cannot be distinguished by the human eye.

To quantify the contrast of intensity we use the definition of the Michelson contrast, which is $(I_{\max} - I_{\min}) / (I_{\max} + I_{\min})$ [22]. I_{\max} and I_{\min} are the highest and lowest luminance. For the PCS investigated in Fig. 2 covered with air compared to pure glycerol we calculate a contrast of 0.54, where I_{\max} and I_{\min} were the spectrally integrated intensity of the resonances in the wavelength range from 530 nm to 610 nm for air and glycerol, respectively. In order to quantify the contrast of hue, first the colors have to be quantified. For this purpose we use the CIE (International Commission on Illumination) color space [23]. In this color space two coordinates (x and y) define the color. x and y are obtained by the convolution of the spectra of interest and the color matching functions, which correspond to the chromatic response of the human eye. An infinitely sharp resonance would be projected on the edge of the CIE color space (spectral locus), whereas an infinitely broad resonance would be positioned in the center of the CIE color space, with the coordinates $x = y = 1/3$. As GMRs have a line-width of only a few nanometers, the calculated color points for the PCS are arranged on a line almost parallel to the spectral locus. The human eye is sensitive to color changes, if the colors are compared side by side, as it is the case in our method. This is defined by the MacAdams ellipses [24], which we exemplarily plotted with 10x magnification around the color point for the PCS with air on its surface. Colors inside this ellipse cannot be distinguished by the human eye from the color in the center. For this PCS we observe that the two color points for air and pure glycerol show a distance, which is about 108 times bigger than the limit defined by the McAdams ellipse.

4. Contrast enhancement of transparent objects in the vicinity of the surface

In a first cell experiment we distributed human epithelial cheek cells on the PCS surface. For an even distribution we placed cells in aqueous solution on the surface of the PCS and allowed the solution to dry. The refractive index of a human epithelial cell is around 1.45, which is comparable to the refractive index of the investigated glycerol.

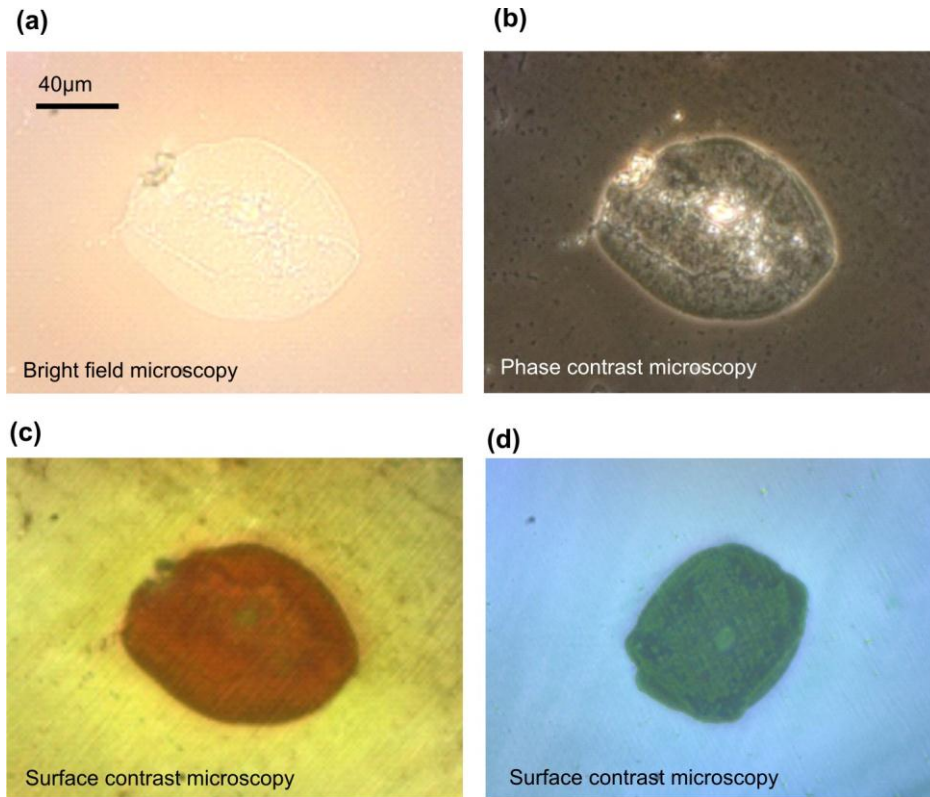


Fig. 3. Human cheek cell on PCS. (a) Bright field microscopy. (b) Phase contrast microscopy. (c) Surface contrast microscopy using a PCS with a periodicity of 370 nm and a 300 nm thick high index layer. (d) Surface contrast microscopy using a PCS with a periodicity of 350 nm and a 135 nm thick high index layer. The color of the PCS with and without object on its surface is a function of the PCS's geometry. Whereas phase contrast microscopy gives overall optical information about the structure of the cell interior, surface contrast microscopy only images the parts of the cell that are close to the surface.

In Figs. 3(a) and 3(b) bright field and phase contrast images of a human cheek cell are shown. Due to the transparency of the cell, the contrast in the bright field mode is low. No effect of the underlying photonic crystal slab is visible. In the phase contrast mode the bright nucleus and the halo effect around the cell allow for a good visibility. However, such a phase contrast image is difficult to evaluate in automated cell recognition systems and tends to be complicated for the calculation of cell parameters, such as cell size, shape, granularity etc. Furthermore, the real contact area between cell and surface is not visible due to the white halo surrounding the cell. In the surface contrast image (Fig. 3(c)), on the other hand, the cell exhibits a contrast of hue and intensity over the entire contact area to the surface and also finer structures from the vicinity of the surface become visible. In particular, the cell edge is very sharply visible. The intrinsic color of the PCS is the result of the spectral position of the GMR provided by the structure. By changing the geometric parameter of the PCS we can tune this color as shown in Fig. 3(d). Here, the PCS was replaced by another PCS composed of a 135 nm indium tin oxide (ITO) layer on a glass substrate with a linear grating (periodicity = 350 nm). We observe a color shift from blue to green and an even a larger intensity decrease.

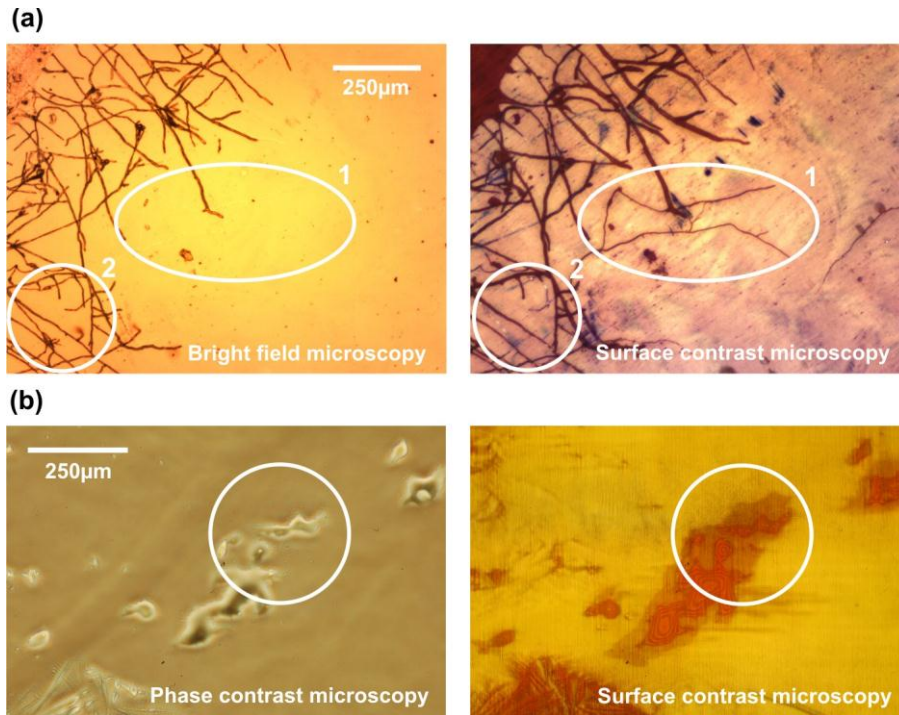


Fig. 4. (a) Mold grown on the surface of the PCS with bright field microscopy and SCM. In area 1 only in the SCM image the transparent part of the mold is visible. In area 2 parts of the mold growing out of the plane exhibit lower contrast enhancement. (b) Lipid remains on the surface of the PCS. Phase contrast microscopy is limited to detecting the thicker parts, surface contrast microscopy also reveals details that are very thin and close to the surface.

As the evanescent part of the QGM is responsible for the contrast, solely objects that are close to the surface experience contrast enhancement. Modes typically extend tens to hundreds of nanometers above the surface. The fungus *Penicillium camemberti* is a mold, which grows as a three-dimensional structure on surfaces and hence is ideal to show this specific characteristic of our method. In Fig. 4(a) we compare a conventional bright field image of the *P. camemberti* with its surface contrast image. As highlighted in area 1, transparent parts of the mold in the vicinity of the surface are visible only in the surface contrast image. On the other hand, in area 2 some part of the mold is growing further away from the surface. This part is not distinguishable from the mold on the surface in the bright field image. In the surface contrast image, however, only a shadow of this part is visible with low contrast. In Fig. 4(b) we demonstrate the sensitivity of our methods to thin, transparent objects on the surface. We compare phase contrast with surface contrast images of lipid drops, which were remains from a spin coating process. Thin details are invisible with phase contrast microscopy, the picture is dominated by the halo effect surrounding thicker structures. Using surface contrast microscopy, however, this part of the object shows a significant contrast enhancement, as highlighted in Fig. 4(b).

The spatial resolution of surface contrast microscopy is a function of the propagation length of the QGM, which is probing the biological tissue [25]. The propagation length is inversely proportional to the dwell time of the photon in the structure and is hence also inversely proportional to the quality factor of the GMR. In [25] the authors demonstrate propagation lengths of down to sub-micron regime and correspondingly high spatial resolution.

5. Homogeneous contrast enhancement for cell segmentation

Another characteristic of surface contrast microscopy is the homogeneous contrast enhancement for the entire object. This characteristic is ideally suited for automated cell detection in microscope images [26]. For cell segmentation we used image data from rat embryonic fibroblast cells grown on the PCS's surface. After fixation, 94 images were taken at random positions using surface contrast microscopy and phase contrast microscopy with a 20x magnification and an image size of 1600x1200 (Fig. 5(a)). To test how a given contrast mechanism helps to improve automated cell segmentation, we successively decreased the pixel resolution by factors of 2 and counted the number of correctly detected cells. All images were scaled down using the pyramid image implementation in MATLAB. To unify all images, background subtraction and image normalization was performed. To evaluate and compare the cell detection performance for both contrast mechanisms, surface contrast and phase contrast, two image segmentation techniques were tested: first, a global threshold segmentation was used to find the cells. This seems an appropriate choice as the resulting data yield a good image contrast. Second, an active contours based cell detection was tested. This segmentation is widely used in cell detection and shows a good performance especially for cell tracking algorithms. To create a ground truth, the cell detection task was performed manually, too. In 12 images the number of cells could not definitely be determined. These images were not used for further evaluation. To assess the detection performance for both image types, the detection error was calculated by $|N_d - N_{gt}| / N_{gt}$, where N_d is the number of cells detected by each segmentation method and N_{gt} is the real number of cells (ground truth).

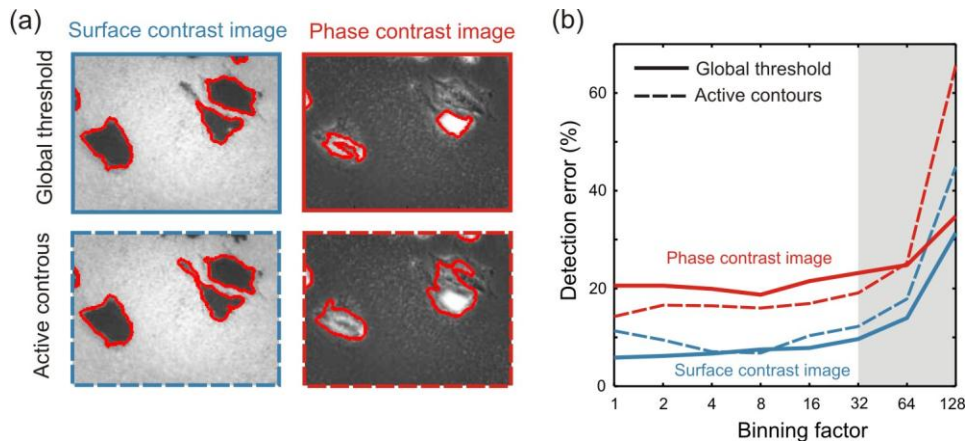


Fig. 5. Qualitative performance comparison of phase contrast microscopy and SCM using automated cell detection. (a) Typical phase contrast microscopy and SCM images with overlaid cell segmentation. (b) Detection error versus binning factor of images for both microscopy methods. Two segmentation methods (global threshold and active contours) were used. The overall error rate for SCM is up to 3.5 times lower using global threshold segmentation and up to 2 times using active contours segmentation compared to phase contrast microscopy. The binning of the image up to a factor of 32 delivers for the global threshold segmentation method error rates below 10%.

The evaluation of both cell detections shows that the global threshold approach is more robust compared to the active contours based segmentation: while the first algorithm could process each image successfully, the active contours based segmentation failed to converge in 10 surface contrast images and in 22 phase contrast images. This high error rate arises from the fact that these algorithms strongly depend on the initial contour; in our case, the initial mask was adjusted to detect cells equally distributed in the image. As a result, all images showing a small number of objects (one up to three cells near the border) were very error-prone, while images with a high cell density could be processed more accurately. A comparison of both segmentation results shows that the detection with surface contrast images outperforms the detection using phase contrast images by a factor of 2.5 to 3.5 (global

threshold) and 1.2 to 2 (active contours) with binning factors from 1 to 32 as depicted in Fig. 5(b). For binning factors beyond 32 the detection error for both methods increases significantly. A binning factor of 32, however, corresponds to an image size of 50x38 pixel and a virtual reduction of the resolution by a factor of 32.

6. Conclusion

In conclusion we present a novel label-free contrast enhancing method for transparent objects and in particular cells on a surface. This method employs PCSs as the microscope slide and can be used with ordinary light microscopes by insertion of only two polarizers. The contrast enhancement on the surface is induced by a superposition of contrast of hue and contrast of intensity, which allows for qualitatively better contrast compared to phase contrast microscopy. The spatial resolution of this method is a function of the modes' quality factor and propagation distance in the PCS rather than the optical limit. In literature sub-micron resolution was demonstrated for a comparable setup [25]. To show also the quantitative superiority of our surface contrast method, we performed automated cell detection in phase contrast microscope and surface contrast images. We observed a significant reduction in the detection error by a factor of up to 3.5 using surface contrast images. Therefore, the technique shown here has the potential to become an important method for imaging cellular processes that occur at or close to the cell-surface contact region.

Acknowledgments

Y. Nazirizadeh and M. Gerken acknowledge support by the German Federal Ministry for Education and Research BMBF (Project No. 03X5514). C. Selhuber-Unkel and J. Reverey acknowledge funding by the Emmy-Noether Programme of the DFG (grant SE 1801/2-1). T. Becker was supported by the Graduate School for Computing in Medicine and Life Sciences funded by Germany's Excellence Initiative [DFG GSC 235/1]. All authors acknowledge support by Deutsche Forschungsgemeinschaft and Open Access Publishing Fund of Karlsruhe Institute of Technology.